Development/Plasticity/Repair

Critical Role of GFRα1 in the Development and Function of the Main Olfactory System

Carolyn Marks,[1,2] **Leonardo Belluscio,**[2] **and Carlos F. Ibáñez**[1,3]

[1]Department of Neuroscience, Karolinska Institute, 17177 Stockholm, Sweden, [2]Developmental Neural Plasticity Unit, National Institute of Neurological Disorders and Stroke, National Institutes of Health, Bethesda, Maryland 20892 , and [3]Life Sciences Institute, Department of Physiology, National University of Singapore, Singapore 117456

Glial cell line-derived neurotrophic factor (GDNF) and its receptor GFRα1 are prominently expressed in the olfactory epithelium (OE) and olfactory bulb (OB), but their importance for olfactory system development is completely unknown. We have investigated the consequences of GFRα1 deficiency for mouse olfactory system development and function. In the OE, GFRα1 was expressed in basal precursors, immature olfactory sensory neurons (OSNs), and olfactory ensheathing cells (OECs), but was excluded from mature OSNs. The OE of newborn *Gfra1* knock-out mice was thinner and contained fewer OSNs, but more dividing precursors, suggesting deficient neurogenesis. Immature OSN axon bundles were enlarged and associated OECs increased, indicating impaired migration of OECs and OSN axons. In the OB, GFRα1 was expressed in immature OSN axons and OECs of the nerve layer, as well as mitral and tufted cells, but was excluded from GABAergic interneurons. In newborn knock-outs, the nerve layer was dramatically reduced, exhibiting fewer axons and OECs. Bulbs were smaller and presented fewer and disorganized glomeruli and a significant reduction in mitral cells. Numbers of tyrosine hydroxylase-, calbindin-, and calretinin-expressing interneurons were also reduced in newborn mice lacking *Gfra1*. At birth, the OE and OB of *Gdnf* knock-out mice displayed comparable phenotypes. Similar deficits were also found in adult heterozygous *Gfra1*$^{+/-}$ mutants, which in addition displayed diminished responses in behavioral tests of olfactory function. We conclude that GFRα1 is critical for the development and function of the main olfactory system, contributing to the development and allocation of all major classes of neurons and glial cells.

Introduction

Neurotrophic factors are secreted proteins with multiple functions in nervous system development, maintenance, and plasticity. Neurotrophic factors play important roles in a variety of fundamental biological processes, such as neurogenesis, neuronal survival, differentiation, migration, axonal growth, synapse formation, and synaptic function. Glial cell line-derived neurotrophic factor (GDNF) was initially discovered as a survival factor for midbrain dopaminergic neurons (Lin et al., 1993). GDNF signals by binding to the glycosylphosphatidylinositol-anchored receptor GFRα1 in complex with the receptor tyrosine kinase RET (Airaksinen and Saarma, 2002). The neural cell adhesion molecule (NCAM) has also been found to mediate biological activities of GDNF in subpopulations of neurons and glial cells in collaboration with GFRα1 (Paratcha et al., 2003). GFRα1 is therefore an essential component of functional GDNF receptors. In addition to midbrain dopaminergic neurons, GFRα1 is expressed by several different classes of neurons and glial cells in both the central and peripheral nervous systems (Trupp et al., 1997; Yu et al., 1998), indicating that GDNF has broader functions than initially proposed.

Our knowledge about the physiological functions and importance of GDNF signaling in the brain is very limited. Although numerous studies have demonstrated the efficacy of exogenous GDNF as a survival factor for midbrain dopaminergic neurons, mice lacking GDNF, GFRα1, or RET do not show any deficits in dopaminergic neuron number, differentiation, or projection at birth (Airaksinen and Saarma, 2002). Moreover, conditional mutants lacking RET in dopaminergic neurons present no major abnormalities up to 1 year of age (Jain et al., 2006; Kramer et al., 2007). Thus, expression of GDNF receptors does not necessarily indicate a requirement of GDNF signaling during development. To date, the only function demonstrated for GDNF during brain development *in vivo* is in the differentiation, migration, and allocation of cortical GABAergic interneurons (Pozas and Ibáñez, 2005; Canty et al., 2009; Perrinjaquet et al., 2011).

The main olfactory system is comprised of two components, the olfactory epithelium (OE) and the olfactory bulb (OB). The OE and OB undergo simultaneous but independent developmental programs during the early formation of the main olfactory system. Expression of GDNF, GFRα1, and RET has been detected in both the OE and OB (Choi-Lundberg and Bohn, 1995; Nosrat et al., 1997; Trupp et al., 1997; Maroldt et al., 2005), but the specific cellular localization of these proteins has not been

Received March 28, 2012; revised Sept. 15, 2012; accepted Sept. 20, 2012.

Author contributions: C.M. and C.F.I. designed research; C.M. performed research; C.M., L.B., and C.F.I. analyzed data; C.M., L.B., and C.F.I. wrote the paper.

This work was supported by grants from the Swedish Research Council, the VIIth Framework Programme of the European Union ("Molpark" network), the Linnaeus Center in Developmental Biology, the Strategic Research Program in Regenerative Medicine (C.F.I.), and the National Institutes of Health (NIH) (L.B.). C.M. was supported by the joint KI/NIH PhD program and the Molpark network. Thanks to Berit Engst, Annika Andersson, Linda Thors, and Sabrina Zechel for assistance.

Correspondence should be addressed to Carlos Ibáñez, Department of Neuroscience, Karolinska Institute, 17177 Stockholm, Sweden. E-mail: carlos.ibanez@ki.se.

DOI:10.1523/JNEUROSCI.1522-12.2012

 0270-6474/12/3217306-15$15.00/0

elucidated. More importantly, despite the abundant expression of these components, the physiological role of GDNF signaling in the olfactory system has not been investigated and remains completely unknown.

In this study, we have mapped the expression of GFRα1 to specific cell types in the developing mouse OE and OB and investigated the consequences of the loss of GFRα1 for the development of these structures in GFRα1 knock-out mice. Our results demonstrate that GFRα1 is critical for the development and function of the main olfactory system, contributing in a dose-dependent manner to the development and allocation of all major classes of neurons and glial cells.

Materials and Methods

Animals

Heterozygous *Gfrα1*$^{+/-}$ (Enomoto et al., 1998) and *Gdnf*$^{+/-}$ (Pichel et al., 1996) mutant mice were bred on a mixed C57/129 and CD1, respectively, genetic background to obtain litters for analysis. Wild-type controls and mutant mice, either knock-outs and/or heterozygous adults, used in the same experiment were always derived from the same litter. For embryonic mice, timed pregnant females (day of vaginal plug equals embryonic day 0.5) were killed by cervical dislocation. Embryonic and newborn pups were swiftly decapitated and placed in 4% paraformaldehyde (PFA) in 0.1 M PBS for either 2 h (for all GFRα1 immunohistochemistry) or overnight (for all other immunohistochemistry) at 4°C. Mice older than postnatal day 0 (P0) were anesthetized with pentobarbital and transcardially perfused with 0.1 M PBS followed by 4% PFA, dissected and postfixed for either 2 h or overnight. All samples were then washed in PBS, cryoprotected in 30% sucrose at 4°C, embedded in OCT compound, snap frozen in a solution of dry ice and 100% ethanol, and finally serially sectioned using a Leica cryostat onto Superfrost Plus (Thermo Fischer Scientific) slides at 20 μm in the coronal plane, air dried and stored at −20°C until use. Additionally, tissue from GAD67-GFP, GAD65-GFP mice (Tamamaki et al., 2003), and OMP-GFP (Potter et al., 2001) were used in this study for GFRα1 coexpression analysis under the same conditions (The Jackson Laboratory). Animal protocols were approved by Stockholm's Norra djurförsöksetiska nämnd and are in accordance with the ethical guidelines of the Karolinska Institute.

In situ *hybridization*

Fresh tissue at P0 and 2 weeks of age was rapidly dissected and snap frozen in OCT embedding medium, and 20 μm coronal sections were collected onto Superfrost Plus slides, using a Leica cryostat, and fixed in 4% PFA for 20 min. *In situ* hybridization was performed using a digoxigenin (DIG)-labeled RNA probe corresponding to the mouse *Gfra1*, *Gdnf*, and *GAP*-43 cDNA C-terminal regions as previously described (Verhaagen et al., 1990; Pozas and Ibáñez, 2005). The slides were hybridized at 65°C overnight. The signal was detected with an alkaline phosphatase-conjugated anti-DIG antibody (Roche) at 4°C followed by NBT/BCIP (Promega) solutions at room temperature.

Immunohistochemistry

Slides were removed from the −20°C, air dried, blocked for 1 h (0.1 M PBS, 5% normal donkey serum, and 0.2% Triton X-100), and incubated in the following primary antibodies (same as block solution) overnight at room temperature: goat anti-GFRα1 (1;200; R&D), rabbit anti-GAP-43 (1;500; Novus Biological), goat anti-OMP (1;5000; Wako Pure Chemicals), rabbit anti-cleaved caspase-3 (1;500; Cell Signaling Technology), mouse anti-Reelin clone G10 (1;300; Millipore), chicken anti-T-box brain (Tbr1) (1:250; Millipore), rabbit anti-calbindin (CB) (1:1000; Millipore), rabbit anti-calretinin (CR) (1:2000; Millipore), rabbit anti-tyrosine hydroxylase (TH) (1:1000; Millipore), rabbit anti-laminin (LN) (1:500; Sigma), rat anti-integrin-α6 (1:500; BD Biosciences), rat anti-NCAM (1:500; BD PharMingen), and guinea pig anti-vesicular glutamate transporter 2 (VGlut2) (1:400; Millipore). After 3 (10 min) washes in PBS, slides were incubated with the following fluorescent secondary antibodies (same diluent as block) for 2 h at room temperature: donkey anti-goat Alexa Fluor 488, 568, or 647; donkey anti-rabbit Alexa Fluor 488, 555, or 647; donkey anti-mouse Alexa Fluor 488, 555, or 647 (all Alexa Fluor secondary's from Invitrogen used at 1:500); donkey anti-rat DyLight 549; donkey anti-chicken DyLight 488; and donkey anti-guinea pig DyLight 549 (all DyLight secondary's from Jackson ImmunoResearch used at 1:400). Finally, slides were washed three times (10 min each) in PBS, 4′-6-diamidino-2-phenylindole (DAPI) 5 mg/ml in PBS (1:10,000; Sigma), and 0.1 M Tris EDTA in H_2O before being air dried and coverslipped in DAKO fluorescent mounting medium.

Bromodeoxyuridine pulse injection

Bromodeoxyuridine (BrdU) (50 mg/kg body weight) in 0.9% NaCl and PBS was injected intraperitoneally in time-mated pregnant mothers at E19. Embryos were collected 2 h after BrdU administration and the standard tissue processing was performed as described above. Sections were incubated in 2N HCl at 37°C for 20 min to denature the DNA, before immunohistochemical staining using a rat anti-BrdU primary antibody (1:500; Accurate Chemical & Scientific) and donkey anti-rat DyLight 549 secondary antibody (1:400; Jackson ImmunoResearch) under the conditions described above.

Imaging and cell counts

All fluorescent images were captured with a Carl Zeiss LSM 710 confocal microscope and ZEN 2009 software. Bright-field images were captured using an upright Carl Zeiss Axioskop microscope, OrcaER digital camera (Hamamatsu), and Openlab software (PerkinElmer). For all cell counts, nine representative images were sampled from the anterior, middle, and posterior regions of the OE or OB for each animal within each group ($n = 10$ for all groups). Within the OE, single optical section (1 μm) images were sampled along the septum. The total number of OMP and GAP43-positive cells per 2 mm and the total number of BrdU and caspase-3 per 4.5 mm were manually counted using Volocity Image Analysis Software (PerkinElmer) and summed per OE for statistical comparison. For all OB cell counts at P0 (Tbr1, Reelin, TH, CB, and CR), low-power confocal *z*-stack images (5 μm thick, at 10× magnification, 0.6 zoom) were collected encompassing the entire OB in each section. Cells were similarly counted using Volocity and summed across the nine images of each OB for each animal and groups. For all cell counts within the adult OB (Reelin, TH, CB, CR), confocal *z*-stack images were captured (20 μm thick, at 10× magnification, 0.7 zoom, 9 mm) along the medial surface, counted, and summed for each OB for comparison within 10 animals for each group.

Glomerular size and number

Nine representative (anterior, middle, and posterior) confocal *z*-stack images (20 μm thick, at 10× magnification, 0.7 zoom, 9 mm) were obtained of the glomerular layer (GL) along the medial surface of each OB from 10 animals at P0 (wild type and null) and 7 weeks of age (wild type and heterozygote) to quantify glomerular size. Glomerular boundaries were defined using three markers: OMP, VGlut2, and DAPI as previously described (Treloar et al., 2009b; Mobley et al., 2010). Glomerular area was measured using the Closed Poly-line tool in ZEN 2009 Light Edition to precisely define the edges of each glomerulus in the *x*, *y*, and *z* planes. Glomerular size values were averaged for each OB and shown as means ± SEM. Glomerular number was calculated by manually counting the total number of glomeruli across nine representative low-power collapsed *z*-stack images for each OB and shown as means ± SD.

Behavioral tests

Buried food test. The test was performed as previously described (Yang and Crawley, 2009). Adult male wild-type and *Gfra1* heterozygous littermate mice (7–10 weeks of age) were tested ($n = 20$ for each genotype). Three consecutive days before the test, mice were given a uniform size palatable food stimulus (Teddy Grahams; Nabisco) as odor familiarization. Mice were food deprived 16 h before testing. Each mouse was then placed into the test cage (46 × 23.5 × 20 cm) containing 3 cm deep clean bedding, for a 5 min acclimation period. Mice were then transferred to an empty clean cage. The food stimulus was placed in a random corner of the test cage 1 cm deep under the bedding and the bedding surface was smoothed out. Mice were placed back in the test cage and the latency was recorded from 2 m away (maximum 15 min) until the mouse found the

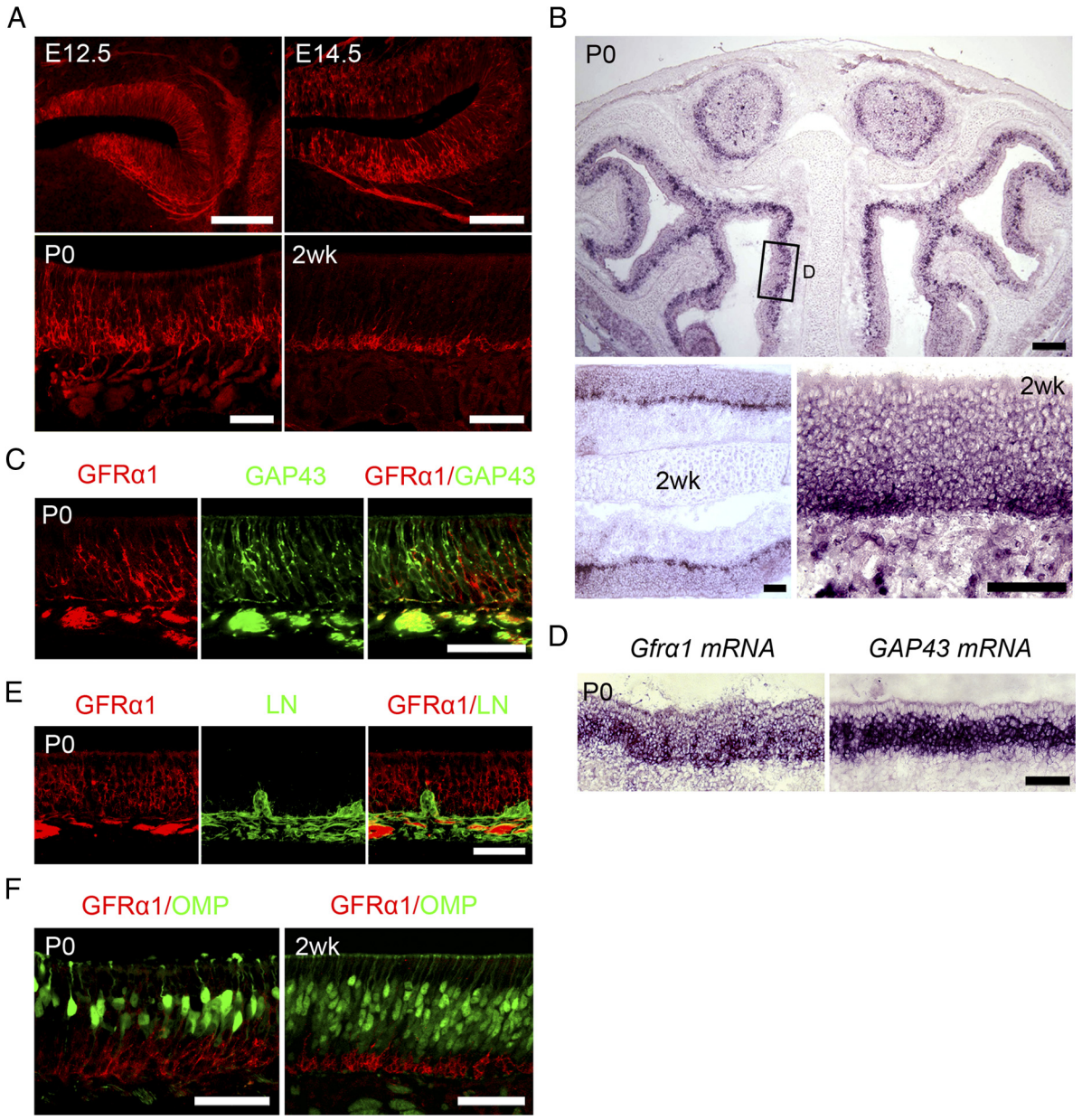

Figure 1. Expression of GFRα1 in the developing mouse OE. ***A***, Overview of GFRα1 expression in the mouse OE at E12.5, E14.5, P0, and 2 weeks as assessed by immunohistochemistry. Scale bars: (E12.5), 100 μm (E14.5), 50 μm (P0), and 50 μm (2 week). ***B***, Expression of *Gfra1* mRNA in the developing mouse OE analyzed by *in situ* hybridization at P0 and 2 weeks. Scale bars: 200 μm (P0), 50 μm (2 week low power), and 50 μm (2 week high power). Box illustrates region in ***D***. ***C***, Expression of GFRα1 in GAP43-positive immature axons and OSNs in the newborn mouse OE. Scale bar, 50 μm. ***D***, Expression of *Gfra1* mRNA in basal cells and GAP-43-positive immature OSNs in the newborn OE. Scale bar, 50 μm. ***E***, Expression of GFRα1 in LN-expressing OECs of the newborn OE. Scale bar, 50 μm. ***F***, At P0 and 2 weeks, GFRα1 did not colocalize with OMP-positive mature OSNs and was restricted to the immature and basal cell layers of the OE. Scale bars: 50 μm (P0 and 2 week).

buried food stimulus. Latency to find the buried food is determined as the time in seconds when the mouse has uncovered the buried food and begins to eat it holding the food with its forepaws. Values are shown as mean latency ± SEM.

Innate olfactory preference and sensitivity tests. Tests were performed as previously published (Kobayakawa et al., 2007; Witt et al., 2009). Adult male wild-type and *Gfra1* heterozygous littermate mice (7–10 weeks of age) were tested only once ($n = 14$ for each genotype and odorant). Mice were individually habituated to the experimental environment for 30 min in a clean empty cage, identical to the test cage, and then transferred to a new cage. Habituation was repeated three additional times. Mice were then transferred to the test cage (20 × 15 × 13 cm) and a filter paper (2 × 2 cm) scented with either water or a test odorant was introduced. Mouse behavior was recorded with a digital video camera for analysis. Investigation times for the filter paper were measured in seconds over a 3 min test period. Investigation was defined by nasal contact with the filter paper within a 1 mm distance. Odorant concentrations used were as follows: distilled water (20 μl), peanut butter (10%w/v, 40 μl), urine of female mice (20 μl), vanillin (64 μM, 20 μl), eugenol (128 μM, 20 μl), 2-methylbutyric acid (2-MB; 8.7M, 20 μl), and trimethyl-thiazoline (TMT; 7.65M, 20 μl). All odorants (Sigma) were dissolved in distilled water except peanut butter, which was dissolved in mineral oil. Values are shown as mean investigation time ± SEM.

Statistical analysis

All graphs and statistics were performed in GraphPad Prism 5.0. A paired Student's *t* test was performed to test statistical significance, assuming a two-tailed distribution and two-sample unequal variance. All values and graphs in all figures are shown as means ± SD (except GL area and behavioral analysis in which a two-tailed unpaired Student's *t* test was

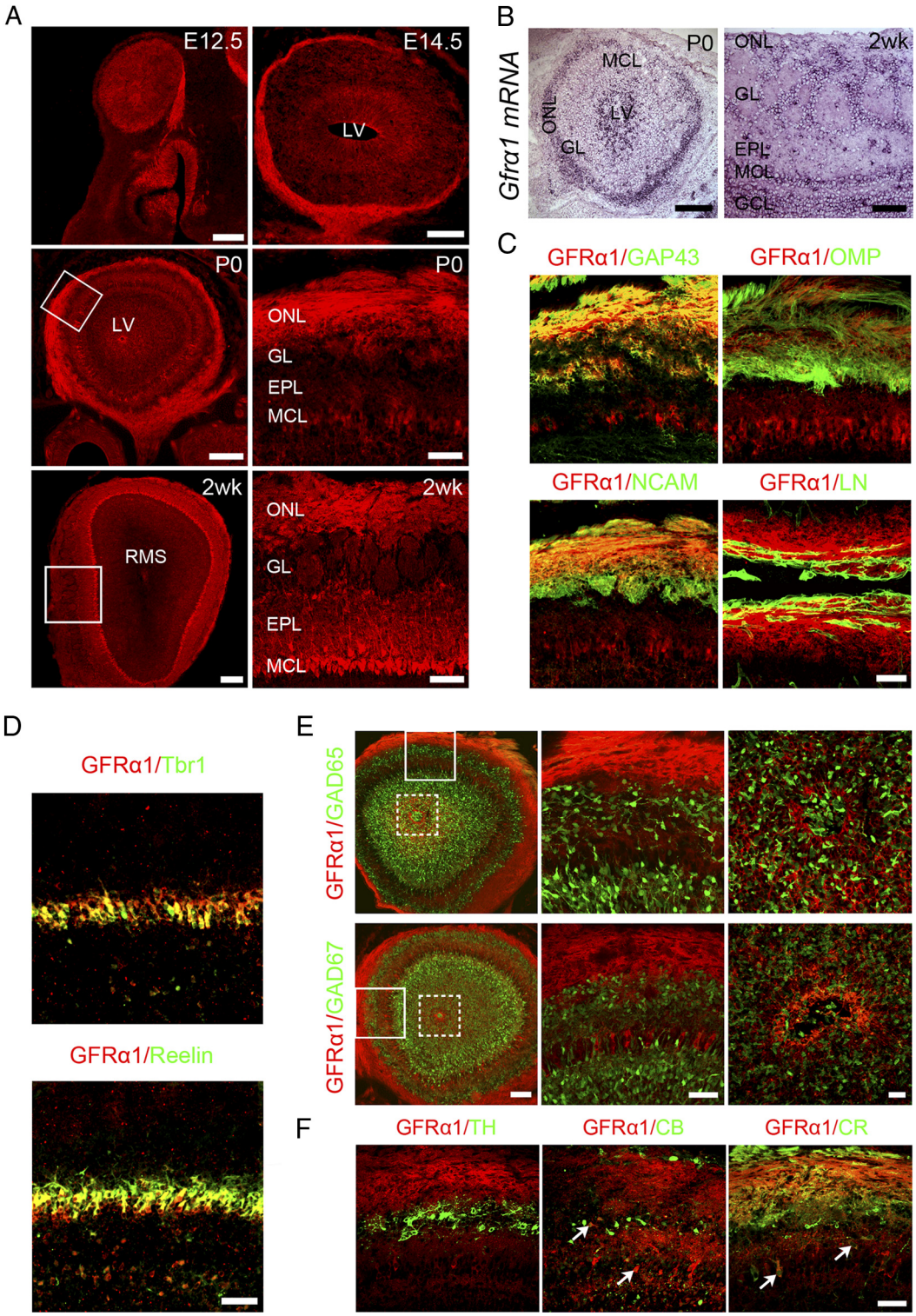

Figure 2. Expression of GFRα1 in the developing mouse OB. ***A***, Overview of GFRα1 expression in the mouse OB at E12.5, E14.5, P0, and 2 weeks assessed by immunohistochemistry. Boxes indicate high-magnification images in P0 and 2 week right panels. Scale bars: 200 μm (E12.5), 100 μm (E14.5), 200 μm (P0 low power), 50 μm (P0 high power), 500 μm (2 week low power), 100 μm (2 week high power). ***B***, Expression of *Gfra1* mRNA in the developing mouse OB analyzed by *in situ* hybridization at P0 and 2 weeks. Scale bars: 200 μm (P0) and 100 μm (2 week). ***C***, Double labeling for GFRα1 and GAP-43 (immature OSN axons), OMP (mature OSN axons), NCAM (all OSNs axons), and LN (OECs) in the ONL of the newborn OB. OMP was detected in OMP-GFP transgenic mice and visualized by GFP fluorescence. The LN panel shows two ONLs from adjacent OBs at the midline. Scale bar, 50 μm. ***D***, Double immunofluorescence for GFRα1 and Tbr1 or Reelin in the newborn OB. Scale bar, 50 μm. ***E***, Lack of colocalization between GFRα1 and GABAergic markers in the newborn OB. GFRα1 (red) was detected by immunohistochemistry in OB from GAD65-GFP and GAD67-GFP transgenic mice as indicated. GAD65 and GAD67 were visualized by GFP fluorescence. Left, Shows whole OB coronal sections. Middle, Shows high-magnification of solid-line boxes. Right, Shows high magnification of dash-line boxes. Size bars; 100 μm (left), 50 μm (middle), 20 μm (right). ***F***, Double immunofluorescence for GFRα1 (red) and interneuron markers TH, CB, and CR (green) in the newborn OB. No overlap was observed with TH. However, a few CB- and CR-positive interneurons colocalized with GFRα1, as depicted by arrows. Scale bar, 100 μm.

performed and average values are shown as means ± SEM); each asterisk indicates a statistically significant p value <0.05.

Results

Cell types expressing GFRα1 in the developing OE

The localization of GFRα1 expression to specific cell types throughout the developing mouse olfactory system was assessed by immunohistochemistry and supplemented by *in situ* hybridization experiments, as indicated. Specific time points were chosen because of their significance within the developmental time line of the olfactory system (Treloar et al., 2009). The specificity of GFRα1 antibodies was validated by comparing wild-type and *Gfra1* knock-out tissue sections. No staining was observed in *Gfra1* knock-out mice with the antibodies used throughout the present study (data not shown). The specificity of the riboprobe used for *in situ* hybridization was also verified by the absence of staining with the corresponding sense probe (data not shown).

The OE, the peripheral component of the main olfactory system, is a pseudostratified neuroepithelium comprised of multiple cell types, including stem and precursor cells in basal layers, immature and mature olfactory sensory neurons (OSNs) in middle and upper layers, respectively, and supporting or sustentacular cells in the most apical layer (Treloar et al., 2009). Basal self-renewing stem cells give rise to a population of transit-amplifying cells that then divide to produce intermediate precursors, the progeny of which differentiates into OSNs (Nicolay et al., 2006; Murdoch and Roskams, 2007). Both immature and mature OSNs express NCAM, but can be distinguished by their differential expression of GAP-43 and olfactory marker protein (OMP), respectively (Farbman and Margolis, 1980; Verhaagen et al., 1989). As OSNs differentiate, they extend axons that cross the underlying OE basal lamina (BL) and navigate toward the rostral telencephalon where the OB forms. Beneath the BL, a heterogeneous population of migratory cells of glial origin, known as olfactory ensheathing cells (OECs), migrates along OSN axons to the OB. OECs envelop OSN axons and can be identified by the expression of different markers, including LN, integrin-α6, and the p75 neurotrophin receptor (Chuah and West, 2002; Whitley et al., 2005). After reaching the olfactory nerve layer (ONL) of the OB, immature OSNs begin to reach into OB glomeruli as they switch off GAP-43 expression, begin expressing OMP, and differentiate into mature sensory neurons (Farbman and Margolis, 1980; Miragall and Monti Graziadei, 1982; Verhaagen et al., 1989).

In the mouse OE, GFRα1 was strongly expressed at E12.5 and E14.5 across the whole epithelium, later coalescing toward the basal half by birth (P0), finally becoming restricted to the most basal region by 2 weeks of age (Fig. 1*A*), where it persisted throughout adulthood. This GFRα1 expression pattern obtained by immunohistochemistry was confirmed by *in situ* hybridization of *Gfra1* mRNA at P0 and 2 weeks of age (Fig. 1*B*,*D*). In the epithelium proper, GFRα1 colocalized with GAP-43 in immature OSNs and their axon bundles beneath the BL at P0 (Fig 1*C*). In agreement with this, *Gfra1 mRNA* was also detected in the immature OSN layer compared with *GAP-43* mRNA, as well as the basal-most portion of the epithelium comprised of basal precursor cells (Fig. 1*D*). Beneath the BL, immunohistochemistry revealed GFRα1 expression in OECs associated with OSN axons, as demonstrated by coexpression with LN (Fig. 1*E*). Interestingly, GFRα1 was excluded from the OMP-expressing mature OSNs that populate the more apical regions of the OE (Fig. 1*F*). After 2 weeks and onward, GFRα1 was clearly restricted to the most basal layers of the OE, excluded

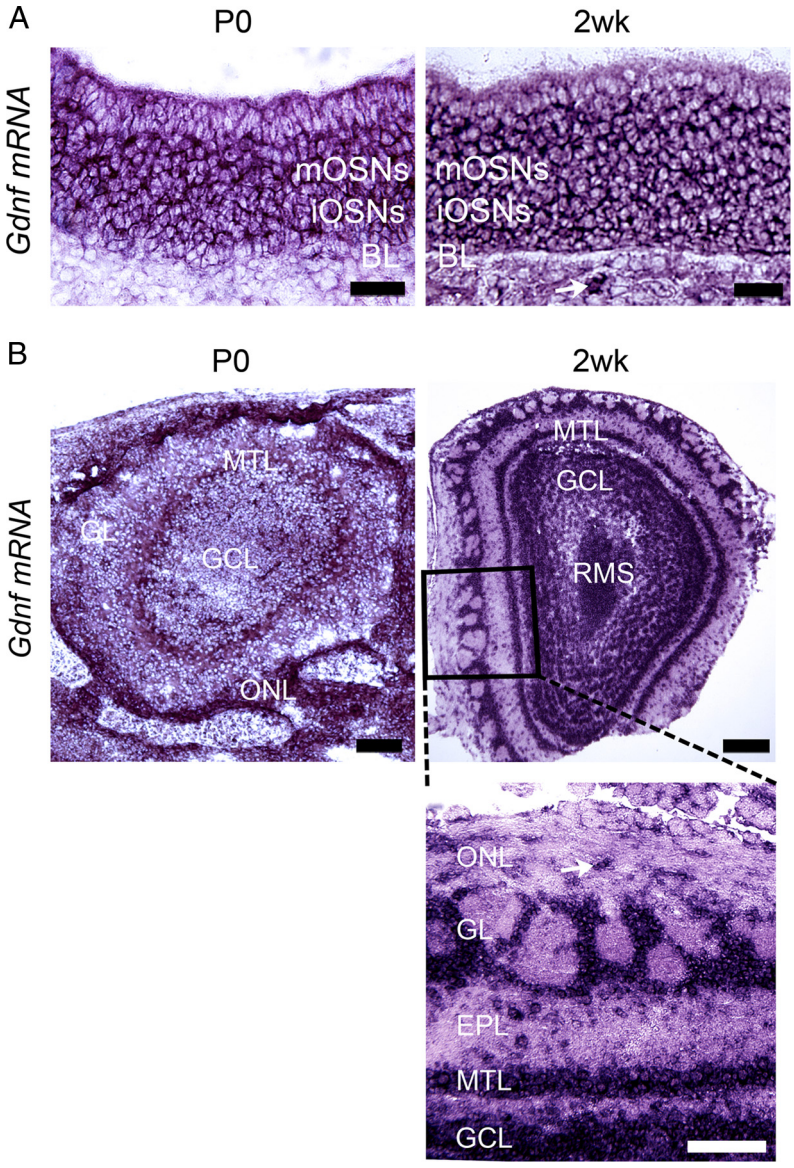

Figure 3. *Gdnf* mRNA expression in the developing olfactory system. ***A***, Expression of *Gdnf* mRNA in the developing mouse OE analyzed by *in situ* hybridization at P0 and 2 weeks. Arrow denotes an OEC expressing *Gdnf* mRNA below the BL. iOSNs, immature OSNs; mOSNs, mature OSNs. Scale bars: 100 μm (P0), 100 μm (2 week). ***B***, Expression of *Gdnf* mRNA in the developing mouse OB analyzed by *in situ* hybridization at P0 and 2 weeks. Arrow denotes OECs expressing *Gdnf* mRNA in the ONL. Scale bars: 100 μm (P0), 200 μm (2 week low magnification), and 100 μm (2 week box, high magnification).

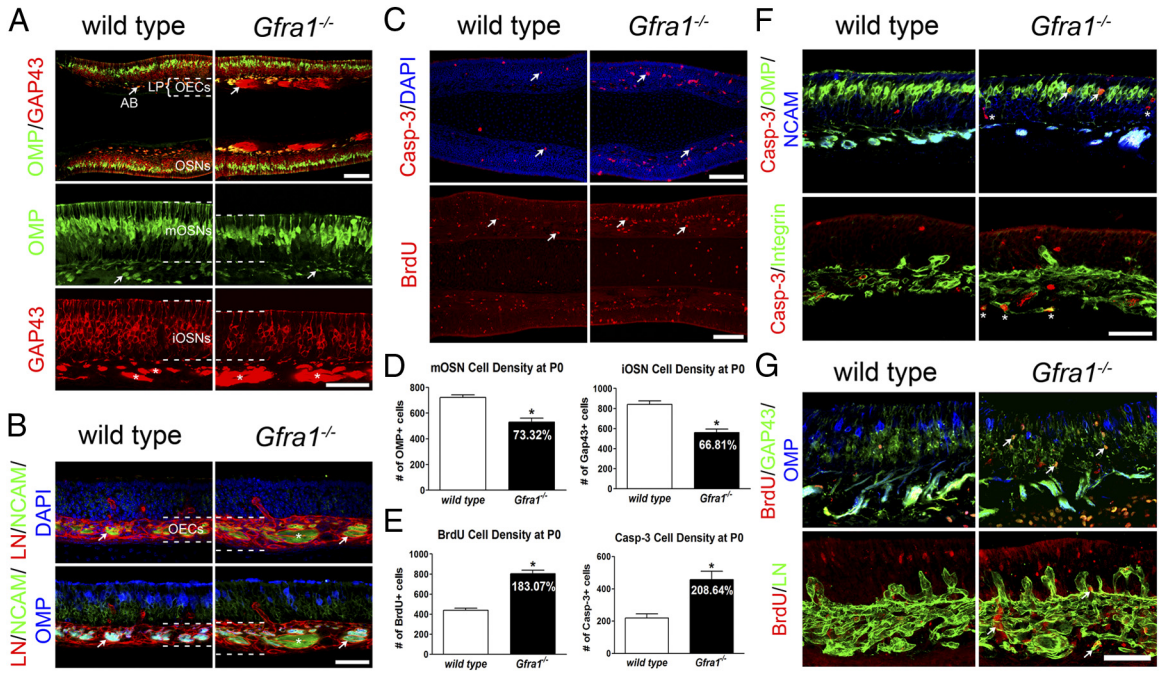

Figure 4. Loss and disorganization of OSNs in the OE of mice lacking GFRα1. ***A***, Mature (OMP, green) and immature (GAP43, red) OSNs and their axons in wild-type and *Gfra1*$^{-/-}$ mutant OE at birth. Arrows denote axon bundles (AB). Asterisks indicate immature ABs. Lamina propria (LP), containing OECs, is marked by dotted lines. Scale bars: 100 μm (top row), 50 μm (bottom row-OMP and GAP-43). iOSNs, immature OSNs; mOSNs, mature OSNs. ***B***, OECs (LN, red), all OSNs (NCAM, green) visualized by immunohistochemistry in newborn wild-type and *Gfra1*$^{-/-}$ mutant OE in relation to all cells (DAPI, blue, top row) or mature OSNs (OMP, blue, bottom row). Arrows depict normal size ABs of mature and immature axons (coexpression of OMP and NCAM). Asterisk denotes enlarged AB in mutant of only immature axons (no coexpression of NCAM and OMP). Scale bar, 50 μm. ***C***, Activated cleaved caspase-3 (arrows) and BrdU incorporation in newborn wild-type and *Gfra1*$^{-/-}$ mutant OE. Counterstaining with DAPI (blue). Arrows indicate the cell types with the greatest increase. Scale bars: 100 μm. ***D***, OMP-positive mature OSN (mOSN) (left) cell density is significantly decreased (*$p < 0.001$, $t = 28.6$) in newborn *Gfra1*$^{-/-}$ mutants (529.7 ± 31.3, $n = 10$) compared with wild-type (722.3 ± 20.6, $n = 10$) per OE. GAP-43-positive immature OSN (iOSN) (right) cell density per OE is dramatically reduced (*$p < 0.0001$, $t = 42.0$) in P0 *Gfra1*$^{-/-}$ mutant (561.6 ± 34.0, $n = 10$) compared with wild-type (840.6 ± 35.0, $n = 10$). Values are mean ± SD. ***E***, Total number of activated caspase-3 cells per OE (right) reveal a significant increase (*$p < 0.0001$, $t = 28.0$) in *Gfra1*$^{-/-}$ knock-outs (457.6 ± 51.3, $n = 10$) compared with control (219.3 ± 26.0, $n = 10$). BrdU incorporating cells (left) are remarkably increased (*$p < 0.0001$, $t = 61.6$) in P0 *Gfra1*$^{-/-}$ mutants (804.9 ± 34.3, $n = 10$) compared with wild-type (439.8 ± 20.9, $n = 10$). Values are mean ± SD. ***F***, Colocalization of activated caspase-3 with NCAM (asterisks in top), OMP (arrows in top) and integrin-α6, an alternative marker of OECs (asterisks in bottom) in the OE of newborn wild-type and *Gfra1*$^{-/-}$ mutants. Scale bar, 50 μm. ***G***, Colocalization of BrdU incorporation with GAP43 (arrows in top), OMP, and LN (arrows in bottom) in the OE of newborn wild-type and *Gfra1*$^{-/-}$ mutants. Scale bar, 50 μm.

from mature, OMP-expressing OSNs that occupy the majority of the OE at those stages (Fig. 1*F*).

Cell types expressing GFRα1 in the developing OB

The OB develops from E12.5 in the mouse as an evagination of the rostral telencephalon. It contains two classes of glutamatergic projection neurons, mitral and tufted cells, and two main classes of inhibitory interneurons, granule cells and periglomerular cells. Projection neurons express Reelin and Tbr1 (Bulfone et al., 1995, 1998; Hurtado-Chong et al., 2009). Apical dendrites from mitral cells coalesce together with incoming axons from OSNs in glomeruli where they form synapses. Inhibitory interneurons form a heterogeneous group, expressing either GAD65 or GAD67, and can be further distinguished by the expression of CB, CR, or TH in mutually exclusive patterns (Parrish-Aungst et al., 2007).

At E12.5 and E14.5, axon bundles reaching the developing OB expressed high levels of GFRα1 as they enveloped the bulb (Fig. 2*A*). By P0, the ONL surrounding the OB was strongly labeled for GFRα1 (Fig. 2*A*). Cells lining the lateral ventricle (LV) were also positive for GFRα1. GFRα1 staining could also be seen in the mitral cell layer (MCL) and the LV at this stage (Fig. 2*A*). At 2 weeks of age, GFRα1 persisted strongly in the ONL and projection neurons of the MCL and external plexiform layer (EPL), and was sparsely expressed in cells associated with the rostral migratory stream (RMS; Fig. 2*A*). This overall pattern was also corroborated by *in situ* hybridization experiments, which also revealed *Gfra1* mRNA expression in cells of the ONL, most likely OECs (Fig. 2*B*). In the ONL of the newborn OB, GFRα1 expression primarily colocalized with GAP-43 in immature OSN axons, but was excluded from mature OSN axons expressing OMP (Fig. 2*C*). In agreement with this, the overlap between GFRα1 and NCAM was partial in the ONL, as NCAM labels both immature and mature OSN axons. GFRα1 immunoreactivity was also seen in LN-expressing OECs of the ONL (Fig. 2*C*), in line with our *in situ* hybridization studies. Moreover, projection neurons of the developing OB also expressed GFRα1, as shown by colocalization with Reelin and Tbr1 (Fig. 2*D*).

No GFRα1 expression could be detected in either GAD65- or GAD67-positive GABAergic interneurons in the newborn OB (Fig. 2*E*). Scattered GFRα1-positive cells could be seen in the glomerular and granule cell layers (GCLs), as well as the central-most portion of the OB, containing the opening of the LV. None of those cells colocalized with GAD65 or GAD67 (Fig. 2*E*). The subpopulation of GABAergic interneurons that express TH, which is almost exclusively GAD67 positive (Choi-Lundberg and Bohn, 1995; Parrish-Aungst et al., 2007), was devoid of GFRα1 expression (Fig. 2*F*, left). Moreover, the great majority of CB- and CR-positive periglomerular interneurons also lacked GFRα1 (Fig. 2*F*). Although a few of those cells did show colocalization with GFRα1 (Fig. 2*F*, arrows), none of them were GABAergic, as they did not coexpress GAD-65 or GAD-67 (data not shown). Non-GABAergic populations of CB- and CR-positive cells have

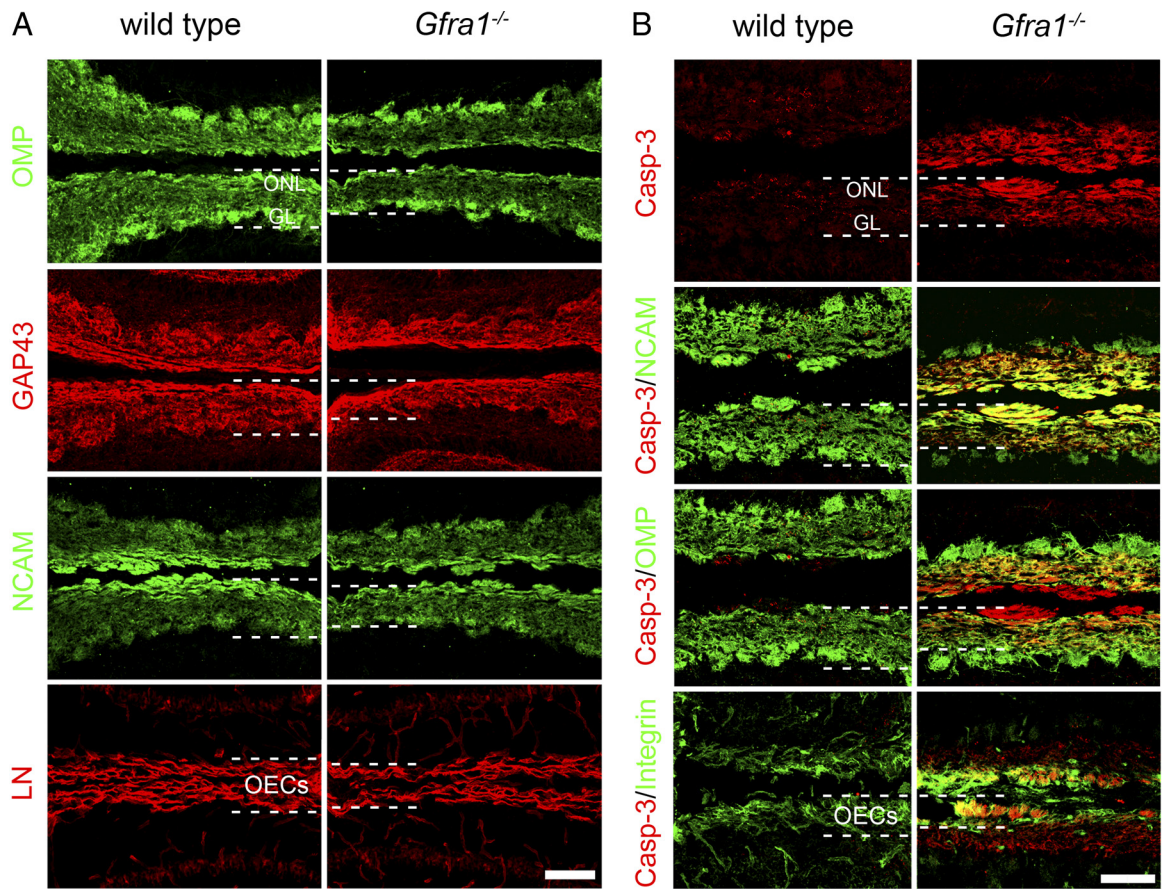

Figure 5. Reduced olfactory nerve layer and loss of OECs in the OB of *Gfra1*$^{-/-}$ mutant mice. ***A***, Immunohistochemistry for OMP, GAP43, NCAM, and LN in the ONL of newborn wild-type and *Gfra1*$^{-/-}$ mutant OBs. ONL thickness is denoted with broken lines and is clearly reduced in mature (OMP), immature (GAP-43), and all OSN axons (NCAM). LN-expressing OECs are also significantly reduced in *Gfra1*$^{-/-}$ mutants, thickness denoted by broken lines of both OBs. Scale bar, 100 μm. ***B***, Colocalization of activated caspase-3 with NCAM, OMP, and integrin-α6 (an alternative marker of OECs) in the ONL of newborn wild-type and *Gfra1*$^{-/-}$ mutant OBs. Scale bar, 100 μm.

previously been described in the mouse OB (De Marchis et al., 2004; Waclaw et al., 2006; Parrish-Aungst et al., 2007), but their developmental origin and function have not been elucidated.

Our findings of the cell types expressing GFRα1 in the main olfactory system contrast with an earlier study that reported GFRα1 expression throughout the whole OE of the adult rat, predominantly in layers corresponding to mature OSNs, and also in OB glomeruli (Maroldt et al., 2005). However, the authors of that report did not perform colocalization studies with either GAP-43 or OMP to precisely localize the GFRα1 signal within the OE, nor with any OB markers. Moreover, we found that the anti-GFRα1 antibodies used in that study produced signals with *Gfra1* knock-out tissue that were indistinguishable from wild type (data not shown). On the other hand, the antibodies used here detected all other major cell populations known to express this receptor, including midbrain dopaminergic neurons, motoneurons, enteric neurons, and kidney nephrons; in all cases labeling was abolished in *Gfra1* knock-out tissue (data not shown).

Gdnf expression in the developing olfactory system

To identify cellular sources of GDNF in the developing mouse olfactory system, we performed *in situ* hybridization studies in newborn and 2-week-old OE and OB. *Gdnf* mRNA expression was detected throughout mature and immature OSN layers in both the newborn and 2-week-old OE (Fig. 3*A*). Below the BL, expression of *Gdnf* mRNA could also be detected in isolated OECs. In the newborn OB, *Gdnf* mRNA expression was most prominent in the MCL, ONL, and scattered cells in the GLs and GCLs (Fig. 3*B*). At 2 weeks of age, strong *Gdnf* mRNA expression could be detected in most cellular elements of the OB, including OECs of the ONL, periglomerular cells, projection neurons in the EPL and MCL, and granule cells (Fig. 3*B*). Abundant *Gdnf* mRNA expression was also observed in the RMS, in agreement with previous observations (Paratcha et al., 2006). Together, these data indicate abundant GDNF expression throughout the developing mouse olfactory system in close proximity to cells and axons expressing the GFRα1 receptor, suggesting a paracrine mode of action.

Loss and disorganization of OSNs in the OE of mice lacking GFRα1

The importance of GFRα1 for the development of the olfactory system was investigated in mice with a global knock-out of this receptor (Enomoto et al., 1998). Homozygous *Gfra1*$^{-/-}$ mutant mice die at birth due to kidney agenesis and defects in the enteric nervous system (Cacalano et al., 1998; Enomoto et al., 1998). Therefore, our analysis of the olfactory system was primarily performed in newborn homozygous mutants. For the OB, some of our studies were also extended to 7-week-old heterozygous mutants (see below).

Inspection of the OE in newborn *Gfra1*$^{-/-}$ mutant mice revealed several morphological abnormalities, in particular, an overall thinning of the epithelium and a dramatic enlargement of

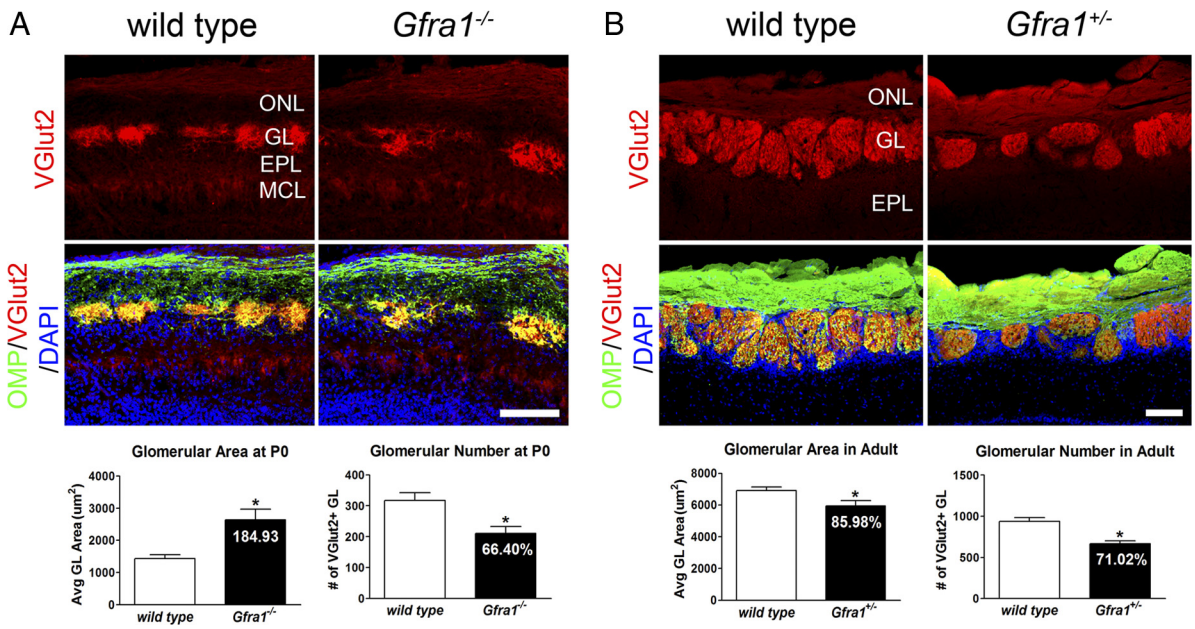

Figure 6. Glomerular deficits in newborn homozygous and adult heterozygous *Gfra1* mutants. ***A***, Glomeruli in wild-type and $Gfra1^{-/-}$ newborn mice were visualized by immunohistochemistry for VGlut2 (red). A superposition with OMP (green) and DAPI (blue) in the bottom was used to define GL boundaries. Scale bar, 100 μm. Histograms show significantly larger ($^*p < 0.0003$, $t = 5.752$) average glomerular area in $Gfra1^{-/-}$ knock-outs (2640 ± 333.7, $n = 570$) compared with controls (1427 ± 128.6, $n = 866$). Values are shown as mean ± SEM. Total number of glomeruli was also reduced ($^*p < 0.0001$, $t = 37.5$) per OB in $Gfra1^{-/-}$ mutants at birth (210.9 ± 22.2, $n = 10$) compared with wild type (317.6 ± 24.7, $n = 10$). Values are shown as mean ± SD). ***B***, Glomeruli of 7-week-old wild-type and $Gfra1^{+/-}$ heterozygous mice. Scale bar, 100 μm. Histograms show significantly smaller ($^*p < 0.0001$, $t = 6.933$) average glomerular area in $Gfra1^{+/-}$ heterozygous mice (5947 ± 332.9, $n = 711$) compared with controls (6916 ± 226.0, $n = 933$). Values are shown as mean ± SEM. Total number of glomeruli were also drastically fewer ($^*p < 0.0001$, $t = 65.39$) per OB in $Gfra1^{+/-}$ heterozygous mice (665.6 ± 35.32, $n = 10$) compared with wild type (937.1 ± 44.82, $n = 10$). Values are shown as mean ± SD.

immature axon bundles (Fig. 4*A*). OMP immunohistochemistry revealed a loss of up to 27% mature OSNs in the mutant OE at birth (Fig. 4*A*,*D*). The distribution of mature OSNs appeared more irregular and disorganized in the OE of $Gfra1^{-/-}$ mutants compared with wild-type controls (Fig. 4*A*). In addition, mature OSN axon bundles were smaller and picnotic in the mutants, both signs of axonal degeneration (Fig. 4*A*, arrows in OMP panels). Immunohistochemistry for GAP-43 revealed a 33% loss of immature OSNs in the mutant OE (Fig. 4*A*,*D*). In contrast to the axon bundles of mature OSNs, however, immature axon bundles were greatly enlarged in the mutants (Fig. 4*A*, asterisks in GAP-43 panel). The enlargement of immature OSN axon bundles was accompanied by an expansion of associated OECs beneath the BL (Fig. 4*B*). Triple labeling for OMP (mature axons), NCAM (all axons), and LN (OECs) clearly demonstrated the specific enlargement of immature axon bundles and increase in associated OECs in the OE of $Gfra1^{-/-}$ mutants at birth (Fig. 4*B*).

Immunostaining for activated caspase-3 revealed a significant increase in apoptosis in the OE of mice lacking GFRα1 (Fig. 4*C*,*E*). Few apoptotic cells were found scattered across all layers of the wild-type OE (Fig. 4*C*). In contrast, the mutant OE showed greater numbers of apoptotic cells, particularly in the more basal layers of the OE, containing immature OSNs and basal precursors, as well as in cells below the lamina propria (Fig. 4*C*). This was confirmed by double immunostaining for OMP (which labels mature OSNs), NCAM (which labels both mature and immature OSNs), and integrin-α6 (which labels OECs). Integrin-α6 immunoreactivity on OECs overlaps with that of LN (Whitley et al., 2005), and was used here due to incompatibility between the animal species of activated caspase-3 and LN antibodies. This analysis showed increase in activated caspase-3 in immature OSNs (i.e., positive for NCAM but negative for OMP), mature OSNs, and OECs (Fig. 4*F*). While immature OSNs and OECs express GFRα1, suggesting cell-autonomous effects in those cells, mature OSNs do not, and hence cell death among this subpopulation is likely due to a noncell-autonomous action (see below). To assess the status of proliferating basal precursors in the wild-type and mutant OE, BrdU was administered to pregnant females at E19 and pups were extracted 2 h later for analysis. We found a dramatic increase in BrdU labeling in the OE of $Gfra1^{-/-}$ mutant mice compared with wild-type controls, particularly among basal precursors (Fig. 4*C*,*E*). Double immunostaining for OMP, GAP43, and LN confirmed increased proliferation of immature OSNs and OECs, but not mature OSNs, in the mutant epithelium (Fig. 4*G*, arrows). The increased number of proliferating basal cells in the OE of $Gfra1^{-/-}$ mutant mice may reflect a defect in their ability to differentiate into OSNs. Alternatively, or in addition, this enhanced proliferation may reflect an attempt to compensate for the loss of OSNs. The increased BrdU incorporation among OECs of $Gfra1^{-/-}$ mutants (Fig. 4*G*, arrows) was in agreement with their increased numbers in the mutant OE.

Reduced ONL and loss of OECs in the OB of $Gfra1^{-/-}$ mutant mice

Newborn mice lacking GFRα1 displayed smaller OBs compared with their wild-type littermates (data not shown). Immunostaining with OMP, GAP-43, and NCAM revealed a thinner ONL in the mutant OB compared with wild-type controls (Fig. 5*A*). The reduction of the ONL was more evident among immature, GAP43-positive OSN axons (Fig. 5*A*) and was accompanied by a significant decrease in LN-expressing OECs (Fig. 5*A*). Thus, while immature axon bundles and OECs appeared enlarged or increased in the mutant OE, they were reduced in the OB, suggesting that GFRα1 is required for appropriate OEC migration

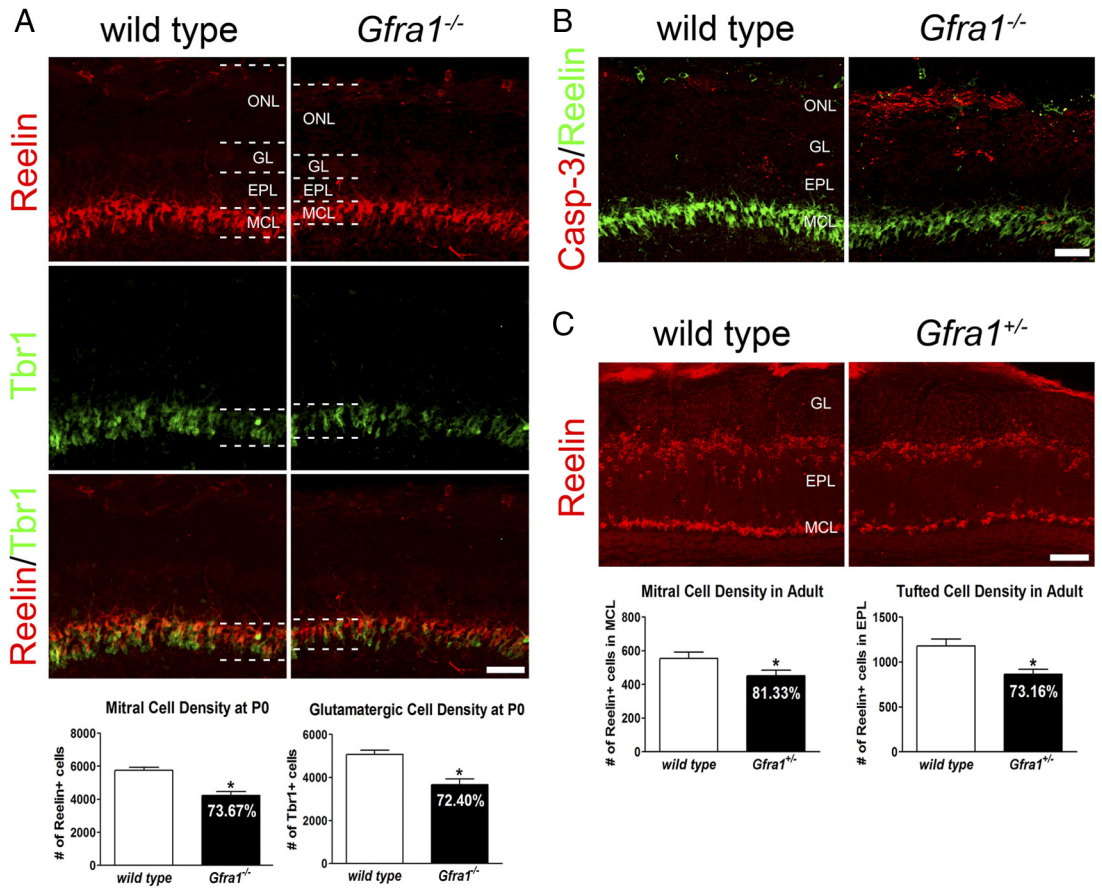

Figure 7. Abnormal distribution and loss of projection neurons in OB of newborn homozygous and adult heterozygous *Gfra1* mutants. ***A***, Immunohistochemistry for Reelin (red) and Tbr1 (green) in OB of newborn wild-type and $Gfra1^{-/-}$ mice. ONL, GL, EPL, and MCL are indicated. Scale bar, 50 μm. Histograms show a significant reduction in both mitral cell density (Reelin-positive cells per OB left, $*p < 0.0001$, $t = 52.8$) and glutamatergic cell density (Tbr1-positive cells per OB right, $*p < 0.0001$, $t = 16.2$) at P0 in $Gfr\alpha1^{-/-}$ mutants (Reelin: 4237 ± 230, $n = 10$;Tbr1: 3674 ± 260, $n = 10$) compared with wild type (Reelin: 5750 ± 194, $n = 10$; Tbr1: 5074 ± 192, $n = 10$). Values are mean ± SD. ***B***, Staining for activated caspase-3 in the newborn OB of *Gfra1* mutant mice does not overlap with Reelin in the mitral cell layer. Scale bar, 50 μm. ***C***, Immunohistochemistry for Reelin in 7-week-old OB of wild-type and $Gfra1^{+/-}$ heterozygous mice. Scale bar, 100 μm. Histograms show significant losses in $Gfra1^{+/-}$ heterozygous mitral cell density (Reelin-positive cells in the MCL, left, $*p < 0.0001$, $t = 37.42$; 450.9 ± 33.26, $n = 10$) and tufted cell density (Reelin-positive tufted cells in the EPL, right, $*p < 0.0001$, $t = 34.25$; 864.0 ± 54.50, $n = 10$) compared with wild type (mitral cell density: 554.4 ± 37.76, $n = 10$; tufted cell density: 1181.0 ± 76.25, $n = 10$). Values are mean ± SD.

and immature OSN axon targeting. The reduction of immature OSN axons and OECs correlated with increased staining for activated caspase-3 in the ONL of the mutants (Fig. 5*B*). Activated caspase-3 was observed predominantly among axons from immature OSNs (Fig. 5*B*), identified here as $NCAM^+/OMP^-$ due to incompatibility between the animal species of activated caspase-3 and GAP43 antibodies. This is in agreement with our OE observations and also in line with a cell-autonomous role for GFRα1 in the maintenance of immature OSN axons. Some $NCAM^-/OMP^+$ axons also showed staining for activated caspase-3 in *Gfra1* mutants (Fig. 5*B*), indicating secondary (i.e., noncell-autonomous) loss of mature OSN axons. Finally, activated caspase-3 was also observed over integrin$^+$ OECs (Fig. 5*B*), in agreement with a cell-autonomous role of GFRα1 in OEC survival.

Glomerular deficits in newborn homozygous and adult heterozygous *Gfra1* mutants

Glomeruli in OB of newborn homozygous $Gfra1^{-/-}$ mutant and wild-type mice were evaluated by immunohistochemistry for VGlut2, which specifically marks glomerular presynaptic terminals from OSN axons (Fig. 6*A*). The OB of $Gfra1^{-/-}$ mutants contained larger, but fewer glomeruli than wild-type controls (Fig. 6*A*). Mutant glomeruli appeared irregularly shaped and disorganized, indicating formation/maturation defects. Strikingly, OB from adult (7 week) heterozygous mutant mice also showed glomerular abnormalities (Fig. 6*B*). In particular, glomeruli were smaller and significantly fewer in heterozygous mutants compared with wild-type controls (Fig. 6*B*). Together, these data suggest a critical, dose-dependent function of GFRα1 in the development and maintenance of olfactory glomeruli.

Abnormal distribution and loss of projection neurons in OB of newborn homozygous and adult heterozygous *Gfra1* mutants

Projection neurons, mitral and tufted cells, were investigated in the OB of *Gfra1* mutant and wild-type mice by immunostaining with antibodies against Reelin and Tbr1. At birth, homozygous *Gfra1* mutants showed fewer Reelin-positive and Tbr1-positive cells compared with wild-type controls (Fig. 7*A*). Both the MCL and the EPL were thinner in these mutants compared with wild-type controls (Fig. 7*A*). Double immunostaining for Reelin and activated caspase-3 did not reveal signs of enhanced apoptosis in the MCL of the mutant OB (Fig. 7*B*), suggesting that the paucity of mitral cells in the mutants may be due to defects in differentiation and/or migration. Tufted cells develop later and occupy

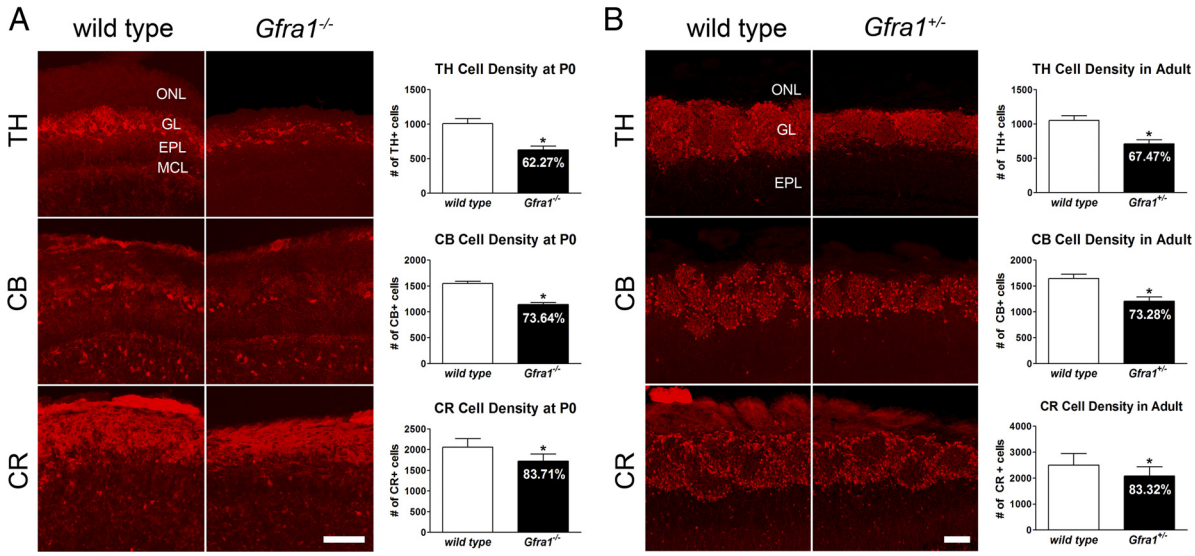

Figure 8. Loss of GABAergic interneurons in OB of newborn homozygous and adult heterozygous *Gfra1* mutants. ***A***, Immunohistochemistry for TH (upper row), CB (middle row), and CR (bottom row) in OB of newborn wild-type and $Gfra1^{-/-}$ mice. ONL, GL, EPL, and MCL are indicated. Scale bar, 100 μm. Histograms show significant losses of TH (*$p < 0.0001$, $t = 36.79$), CB (*$p < 0.0001$, $t = 33.19$), and CR (*$p < 0.0001$, $t = 14.56$) in $Gfra1^{-/-}$ mutants (TH: 628.7 $\pm$ 52.29, CB: 1141 $\pm$ 36.45, and CR: 1721 $\pm$ 172.2, $n = 10$ for all groups) compared with controls (TH: 1010 $\pm$ 70.43, CB: 1550 $\pm$ 43.02, and CR: 2056 $\pm$ 207.8, $n = 10$ for all groups). Images are high-power representation of results. Values are mean $\pm$ SD. ***B***, TH-, CB-, and CR-expressing interneurons in 7-week-old OB of wild-type and $Gfra1^{+/-}$ heterozygous mice. Scale bar, 100 μm. Histograms show quantification of TH, CB, and CR cell density. $Gfra1^{+/-}$ heterozygous mice have significantly fewer TH (*$p <$ 0.0001, $t = 21.05$; 709.6 $\pm$ 58.58), CB (*$p < 0.0001$, $t = 38.81$; 1207 $\pm$ 80.44), and CR (*$p < 0.0001$, $t = 11.39$; 2081 $\pm$ 354.1) interneurons compared with wild type (TH: 1052 $\pm$ 70.19, CB: 1647 $\pm$ 79.15, and CR: 2498 $\pm$ 446.8, $n = 10$ for all groups). Values are shown as mean $\pm$ SD. Scale bar, 100 μm.

positions above the MCL in the EPL, as visualized by immunostaining for Reelin (Fig. 7*C*). At 7 weeks of age, heterozygous *Gfra1* mutants showed reduced numbers of both mitral and tufted cells compared with wild-type controls (Fig. 7*C*), indicating a dose-dependent function of GFRα1 in the development of OB projection neurons.

Loss of GABAergic interneurons in OB of newborn homozygous and adult heterozygous *Gfra1* mutants

The OB from both newborn homozygous and 7-week-old heterozygous *Gfra1* mutants presented significant losses of periglomerular and granule cell interneurons. The most pronounced deficit (30–40% loss) was among TH-expressing neurons, followed by CB-expressing neurons (27% loss) and CR-expressing neurons (17% loss) (Fig. 8*A*,*B*). Relative interneuron losses were comparable in P0 and 7-week-old mutant animals, suggesting that GFRα1 functions in a dose-dependent manner to regulate the allocation and/or maintenance of interneurons in the OB throughout postnatal development. Activated caspase-3 immunoreactivity was very sparse in periglomerular and granule cell layers of both wild-type and mutant OB (data not shown), indicating that loss of interneurons in *Gfra1* mutants may be the result of impaired differentiation or migration from their sites of origin. Our expression studies (see above) indicated that GFRα1 did not colocalize with either GAD65 or GAD67, the two main GABAergic markers, and was not present in TH-positive interneurons. Although a very small fraction of CB- and CR-expressing cells appeared to be positive for GFRα1, none of those cells expressed GAD65 or GAD67. The very limited number of CB- and CR-positive cells that coexpressed GFRα1 could not account for the losses observed among CB and CR cell subpopulations in the mutant OB, suggesting that many interneurons that do not normally express GFRα1 were lost in the mutants. This situation is analogous to the loss of parvalbumin-expressing interneurons observed in the cerebral cortex of *Gfra1* mutant mice, which do not themselves express this receptor (Pozas and Ibáñez, 2005; Canty et al., 2009).

Similar deficits in the olfactory system of newborn mice lacking GDNF

To verify whether loss of GDNF leads to phenotypes similar to those observed in *Gfra1* mutants, we performed a limited survey of mature and immature OSNs, ONL, and OB GABAergic interneurons in the olfactory system of newborn *Gdnf* knock-out mice. At birth, $Gdnf^{-/-}$ mutant mice displayed a thinner OE with paucity of both mature and immature OSNs and enlarged $GAP43^{+}$ axon bundles, all phenotypes shared by *Gfra1* knock-out mice (Fig. 9*A*). In the OB, newborn $Gdnf^{-/-}$ mice displayed a significantly reduced ONL and irregularly shaped glomeruli (Fig. 9*B*). Further analysis of GABAergic interneurons revealed reductions in the number of TH-, CB-, and CR-expressing cells in the OB of newborn mice lacking GDNF (Fig. 9*C*), also in agreement with our observations in *Gfra1* mutants. Interestingly, interneuron losses in OB of $Gdnf^{-/-}$ and $Gfra1^{-/-}$ mice were remarkably similar, indicating that GDNF may be the main ligand driving GFRα1-mediated effects in OB interneurons. Together, these studies suggest similar deficits in the olfactory systems of the two mutants at birth.

Behavioral tests of olfactory function reveal impaired olfactory responses in adult heterozygous *Gfra1* mutants

The unexpected neuroanatomical deficits of the olfactory system of adult heterozygous *Gfra1* mutants prompted us to examine olfactory function in these animals. Behavioral responses to odors were investigated using standardized tests of olfaction. In the buried food assay, animals search for a pellet of highly palatable food buried in cage bedding after having been subjected to a period of food restriction (Yang and Crawley, 2009). Olfactory disability has been shown to significantly impair performance in this assay, resulting in longer latencies to food pellet retrieval.

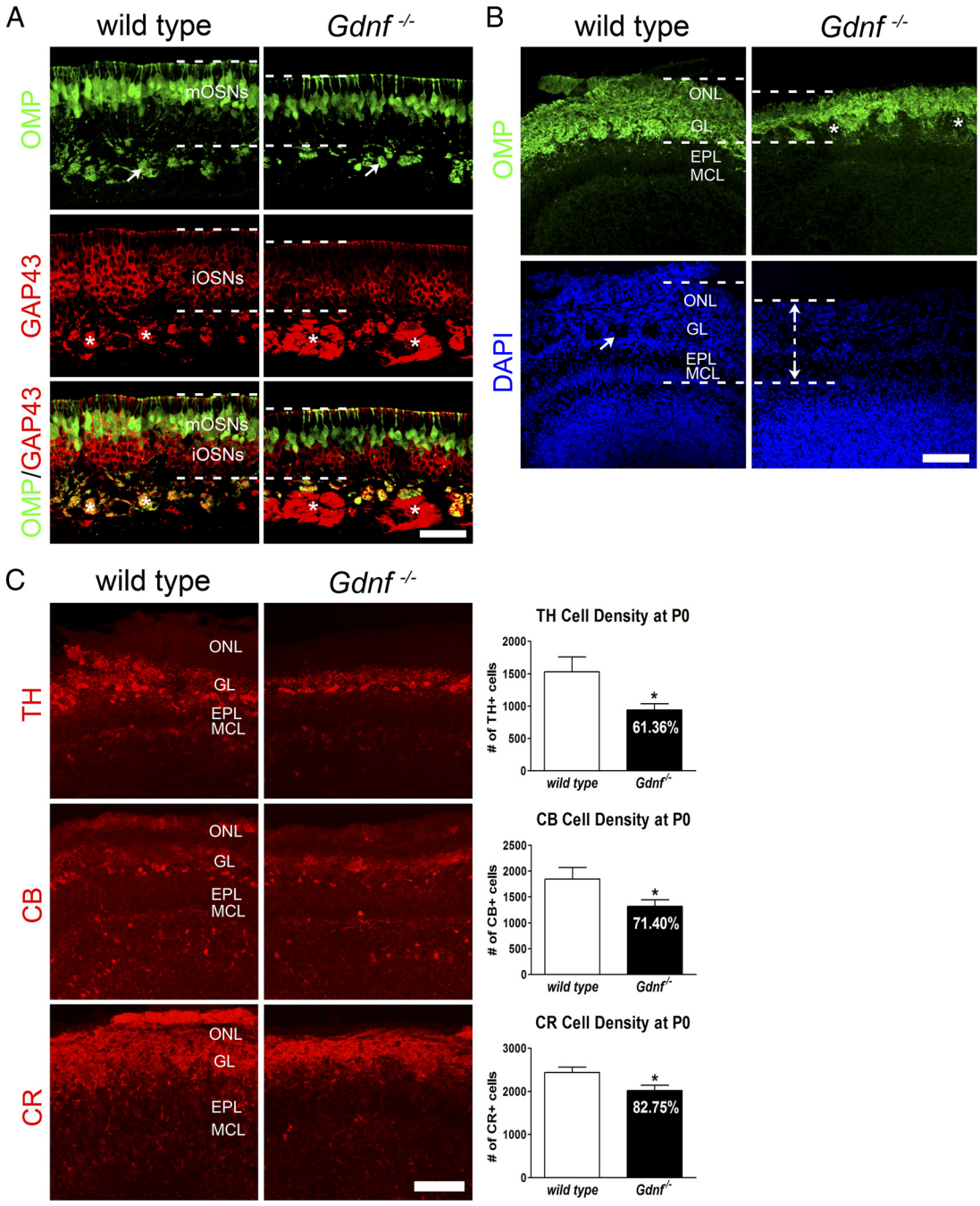

Figure 9. Deficits in the olfactory system of newborn mice lacking GDNF. ***A***, Mature (OMP, green) and immature (GAP43, red) OSNs and their axons in wild-type and $Gdnf^{-/-}$ mutant OE at birth. Arrows denote mature axon bundles. Asterisks indicate immature axon bundles. Lamina propria is marked by dotted lines. Scale bar, 50 μm. ***B***, Immunohistochemistry for OMP (green, top) in the ONL of newborn wild-type and $Gdnf^{-/-}$ mutant OBs. ONL/GL thickness is denoted with broken lines and is clearly reduced in $Gdnf^{-/-}$ mutants. Asterisks denote irregularly shaped glomeruli in the mutants. DAPI staining (blue, bottom) shows the reduction in OB layers of newborn $Gdnf^{-/-}$ mutant mice. Arrow indicates round discrete glomeruli in wild type. Scale bar, 100 μm. ***C***, Immunohistochemistry for TH (upper row), CB (middle row), and CR (bottom row) in OB of newborn wild-type and $Gdnf^{-/-}$ mice. ONL, GL, EPL, and MCL are indicated. Histograms show quantification of TH, CB, and CR cell density. Newborn $Gdnf^{-/-}$ mutant mice have significantly fewer TH ($^*p < 0.0001$, $t = 13.75$; 940.0 ± 97.96), CB ($^*p < 0.0001$, $t = 9.548$; 1317 ± 127.5), and CR ($^*p < 0.0001$, $t = 20.89$; 2021 ± 122.2) interneurons compared with wild type (TH: 1532 ± 228.3, CB: 1844 ± 226.7, and CR: 2443 ± 117.5, $n = 10$ for all groups). Values are shown as mean $\pm$ SD. Scale bar, 100 μm.

Adult heterozygous *Gfra1* mutants displayed considerably longer latencies compared with wild-type mice in this assay (Fig. 10*A*), suggesting a diminished olfactory response. For a more specific assessment of olfactory function, mutant and wild-type animals were subjected to a combined innate olfactory preference and sensitivity test. In this assay, a mouse is presented with a defined odor spotted on a piece of filter paper and the time that the mouse spends investigating the paper is recorded. Different groups of mice are presented with different odors known to elicit innate responses, i.e., attractive, neutral, and aversive, respectively; each animal is exposed to only one odor during the test (Kobayakawa et al., 2007; Witt et al., 2009). Water typically results in investigation times of ~4 s and this is taken as the neutral response threshold (Fig. 10*B*). Attractive odors, such as peanut butter and urine

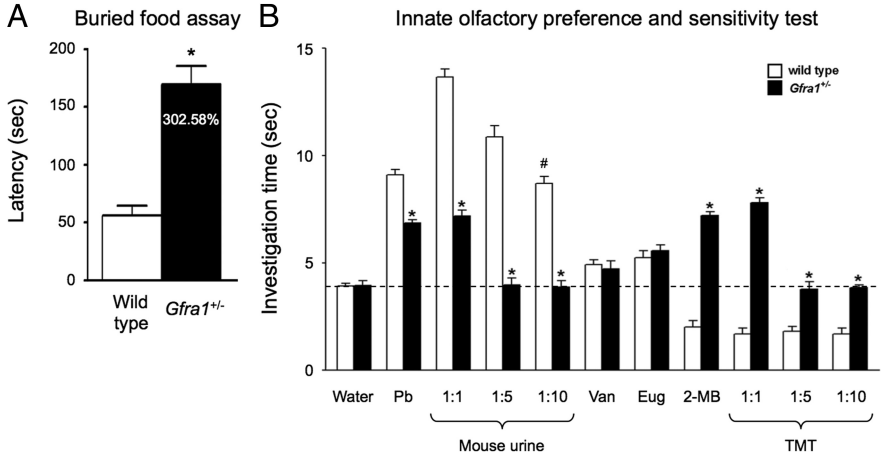

Figure 10. Impaired olfactory function in heterozygous *Gfra1* mutants. ***A***, Buried food assay. Adult male heterozygous *Gfra1* mutant mice displayed a significantly (*$p < 0.0001$, $t = 6.286$) longer latency measured in seconds (56.10 ± 8.51, $n = 20$) to retrieve a buried food pellet compared with wild-type controls (169.8 ± 15.95, $n = 20$). Values are shown as mean latency in seconds ± SEM. ***B***, Innate olfactory preference and sensitivity test. Histogram depicts the duration in which wild-type and *Gfrα1* heterozygous mice investigated a scented filter paper with various odorants measured over a 3 min test period. All odorants tested at concentrations given in Material and Methods (1:1); female mouse urine and TMT were also tested at 1:5 and 1:10 dilutions. Dotted line denotes the neutral level of response (water). *$p < 0.0001$ versus wild type for each odor; #$p < 0.0001$ versus wild-type water, $n = 14$ for each genotype and odorant. Values are shown as mean investigation time in seconds ± SEM.

of the opposite sex, elicit longer investigation times, while aversive odors, such as 2-MB (pungent odorant of spoiled foods) and TMT (a component of fox urine), result in shorter investigation times compared to water. Neutral odors, such as vanillin and eugenol, do not elicit an innate olfactory response in mice and so result in investigation times comparable to that of water. Wild-type male mice reacted as expected, displaying longer investigation times to peanut butter and female mouse urine; similar times for water, vanillin, and eugenol; and shorter times for 2-MB and TMT (Fig. 10*B*). Heterozygous *Gfra1* mutants also showed normal responses to water and neutral odors. However, they displayed significantly reduced investigation times to attractive odors compared with wild-type mice (Fig. 10*B*). Importantly, the response of heterozygous mutants to mouse urine dropped to the neutral level after a 5-fold dilution of the odorant, while wild-type animals continued to show attractive responses up to a 10-fold dilution (Fig. 10*B*). These results are indicative of diminished olfactory sensitivity in the mutants.

The response of heterozygous *Gfra1* mutants to aversive odors was more complex. At high concentrations, investigation times for 2-MB and TMT were longer than that for water, comparable to those shown for attractive odors peanut butter and female urine, and much longer than the investigation times shown by wild-type mice (Fig. 10*B*). Although this result may at first appear puzzling, data from behavioral tests should be interpreted with caution as it is known that behavioral responses to odorants are affected by their concentrations. There is a well known trade-off between speed and accuracy in rodent olfactory recognition (Abraham et al., 2004; Rinberg et al., 2006); hence it is possible that heterozygous *Gfra1* mutants require more time to recognize the qualities of aversive odors in the innate preference test as a consequence of diminished olfactory sensitivity. In line with this possibility, the response of the mutants to TMT became indistinguishable from that to water after a 5-fold dilution, while wild-type mice remain equally averse to both 5- and 10-fold dilutions of this odorant (Fig. 10*B*), indicating a reduced detection threshold in the mutants. Together, these results indicate impaired olfactory responses in adult heterozygous *Gfra1* mutant mice and reinforce the important role of GFRα1 in the development and function of the olfactory system.

Discussion

In this study, we have identified the precise cellular distribution of GFRα1 in the epithelium and bulb of the main olfactory system using specific cell markers, and investigated the importance of GFRα1 for olfactory system development in mutant mice in which GFRα1 expression was either absent or diminished. Our findings revealed a critical role for GFRα1 in the development of several of the major cell types of the main olfactory system, including OSNs, OECs, projection neurons, and inhibitory interneurons.

The OE of mice lacking GFRα1 was thinner, contained fewer OSNs, and showed increased levels of cleaved caspase-3 compared with wild-type controls. Thus, GFRα1 may function cell autonomously in immature OSNs to regulate their differentiation and survival. It is also possible that fewer OSNs are being generated in the mutants due to defects in stem cell differentiation and OSN neurogenesis. In line with this, we observed increased BrdU labeling in the basal portion of the OE of mice lacking GFRα1. The increase in basal cell proliferation in the mutants may also reflect an attempt to compensate for the loss of OSNs. Distinguishing between these possibilities will require selective inactivation of GFRα1 expression in OE stem cells, immature OSNs, and OB targets.

Axon bundles of immature, GAP-43-expressing OSNs were dramatically enlarged and associated OECs were increased in the mutant OE. This contrasted with a clear reduction in ONL thickness, GAP-43-positive axons, and OECs in the OB of the mutants, suggesting that a fraction of immature OSN axons and OECs fail to migrate to the OB and are instead stalled in the OE in the absence of GFRα1. *In vitro* studies have shown that GDNF signaling can promote OEC migration (Cao et al., 2006; Treloar et al., 2009b; Mobley et al., 2010) and that migration of OECs stimulates OSN growth cone activity and axon extension (Treloar et al., 2009a; Windus et al., 2011). It is therefore possible that the loss of GFRα1 from OECs affected their motility, leading to accumulation of OECs and immature axons in the OE and a corresponding reduction in the OB. An abnormal excess of OECs may lead to apoptosis of some of these cells and account for the increased activation of caspase-3 observed in cells below the BL in the mutant OE. Given that GFRα1 was also expressed in immature OSN axons, GDNF signaling may also directly influence OSN axon growth independently of its effects on OECs. The relationship between OECs and OSN axons is complex and has not yet been elucidated in an *in vivo* setting. Selective elimination of GFRα1 in immature OSN axons or OECs should allow its direct effects on these cell types to be distinguished and shed light onto the relationship between OECs and OSN axons *in vivo*.

Although mature OMP-positive OSNs did not express GFRα1, their reduced numbers in *Gfra1* knock-out mice are consistent with a reduction in the pool of immature OSNs from which they arise. Some of the remaining mature OSN in the

mutants showed enhanced apoptosis and signs of axonal degeneration, suggesting a noncell-autonomous effect of the loss of GFRα1. This could be a result of the loss of OSN targets in the OB, particularly mitral cells, which appeared severely affected in the mutants (see below).

GDNF signaling is required for the maintenance of the ONL, as mutants lacking GFRα1 showed reductions in OSN axons and OECs and increased activation of caspase-3. Several caspases, including caspase-3, have been detected in axons and dendrites of different classes of CNS neurons, including OSN axons (Verhaagen et al., 1990; Cowan et al., 2001; Cowan and Roskams, 2004). Earlier studies proposed that caspase-3 participates in a retrograde pro-apoptotic signal from synapses to cell bodies in developing OSNs (Cowan et al., 2001; Cowan and Roskams, 2004). The increase in caspase-3 activity detected in the ONL of mice lacking GFRα1 would thus be consistent with the reduced OSNs observed in the mutant OE. More recently, roles for caspases independently of cell body apoptosis have begun to emerge. The participation of caspase-6 in axonal degeneration has been demonstrated in several recent studies (Nikolaev et al., 2009; Park et al., 2010). Although the requirement for caspase-3 in axonal degeneration remains controversial (Nikolaev et al., 2009; Schoenmann et al., 2010), local upregulation of caspase-3 activity has recently been linked to functional and structural alterations in synapses (Li et al., 2010; D'Amelio et al., 2011). These and other data suggest that elevated caspase-3 activity in the ONL of mice lacking GFRα1 could also reflect a higher turnover of immature OSN axons in the mutants.

The deficits observed in the two major components of OB glomeruli, namely OSN axons and mitral cell dendrites, are likely to account for the glomerular abnormalities in the OB of *Gfra1* mutants. GFRα1 has been shown to display synaptogenic activity in developing neurons of the hippocampus and cerebral cortex through a process called ligand-induced cell adhesion (Ledda et al., 2007). In addition to a paucity of OSN axons and mitral cells, GDNF signaling might also be necessary for the initial synapse formation/stabilization that occurs just as immature OSNs are transitioning to mature OSNs (Carson et al., 2005).

Significant defects were also observed among different classes of inhibitory interneurons expressing CB, CR, and TH in OB lacking GFRα1. Loss of GFRα1 could affect olfactory interneuron development noncell autonomously as a consequence of defects in OSNs and projection neurons (De Carlos et al., 1995; Gong and Shipley, 1995; Bulfone et al., 1998; Treloar et al., 2009a). Alternatively, GFRα1 may also be important for the development of OB interneuron precursors. These cells are generated in the lateral ganglionic eminences, subventricular zone, and septum of the embryonic forebrain, and migrate rostrally to the OB through the lateral ventricle and a cell migration pathway known as the RMS (Luskin, 1993, 1998; Lois and Alvarez-Buylla, 1994; Wichterle et al., 2001). GFRα1 colocalizes with NCAM in RMS cells (Paratcha et al., 2003) and GDNF has been shown to function as a chemoattractant factor for these cells in a NCAM-dependent manner (Paratcha et al., 2006). GFRα1 could thus function cell autonomously in subpopulations of OB interneuron precursors to regulate their differentiation, migration, or survival before their final allocation in the OB.

Several of the phenotypes observed in newborn *Gfra1* knockout mice, including thinning of the OE, paucity of OSNs, enlarged GAP43$^+$ axon bundles, reduced ONL, irregularly shaped glomeruli, and decreased number of all major classes of GABAergic interneurons, were also reproduced in newborn pups lacking GDNF. The similarities between the phenotypes of the two mutants suggest that GDNF may be the main ligand driving GFRα1-mediated effects in olfactory system development.

The olfactory system undergoes significant development during postnatal stages until approximately the seventh week after birth in the mouse (Treloar et al., 2009a). Mice homozygous for a null mutation in G*fra1* die at birth due to kidney agenesis and defects in the enteric nervous system (Cacalano et al., 1998; Enomoto et al., 1998). Although heterozygous mutants survive birth, GFRα1 has not been known to display dose-dependent effects *in vivo*, and no developmental abnormalities have been described in heterozygous *Gfra1* mutants. We were therefore surprised to find such dramatic defects in these animals, highlighting the exquisite sensitivity of the olfactory system to GFRα1 dosage and the critical role of this receptor in its development. Remarkably, interneuron losses were proportionally comparable in newborn homozygous and adult heterozygous mutants, suggesting that OB interneurons are critically dependent on GFRα1 during postnatal stages. This is in agreement with the continuous replenishment of this neuronal subpopulation from RMS precursors throughout life (Hinds, 1968a, b; Bayer, 1983). The pronounced neuroanatomical deficits of the olfactory system of adult *Gfra1*$^{+/-}$ mutants correlated with a decreased olfactory sensitivity in both the buried food assay and innate olfactory sensitivity test. Abnormal innate responses to aversive odorants similar to those observed here have also been described as a result of OSN ablation (Kobayakawa et al., 2007) and lack of Robo-2 in OSNs (Cho et al., 2011). Given the broad effects of GFRα1 throughout the olfactory system, it cannot be ruled out that some of the behavioral responses of *Gfra1* mutants, particularly those elicited by aversive odors, may be a consequence of disordered OB circuitry in addition to diminished sensitivity.

In summary, this study demonstrates that GFRα1 is critical for the development of all major classes of neurons and glial cells in the main olfactory system. It provides the groundwork for future studies focused on the different functions of this receptor in the individual neuronal and glial cell types that comprise the olfactory system. Important questions to address include the cell-autonomous and noncell-autonomous mechanisms by which GFRα1 orchestrates olfactory system development, its role in precursors versus mature cells, its effects on synaptic connectivity, and the differential contributions of GFRα1 coreceptors to the functions described here.

References

Abraham NM, Spors H, Carleton A, Margrie TW, Kuner T, Schaefer AT (2004) Maintaining accuracy at the expense of speed: stimulus similarity defines odor discrimination time in mice. Neuron 44:865–876. CrossRef Medline

Airaksinen MS, Saarma M (2002) The GDNF family: signalling, biological functions and therapeutic value. Nat Rev Neurosci 3:383–394. CrossRef Medline

Bayer SA (1983) 3H-thymidine-radiographic studies of neurogenesis in the rat olfactory bulb. Exp Brain Res 50:329–340. Medline

Bulfone A, Smiga SM, Shimamura K, Peterson A, Puelles L, Rubenstein JL (1995) T-brain-1: a homolog of Brachyury whose expression defines molecularly distinct domains within the cerebral cortex. Neuron 15:63–78. CrossRef Medline

Bulfone A, Wang F, Hevner R, Anderson S, Cutforth T, Chen S, Meneses J, Pedersen R, Axel R, Rubenstein JL (1998) An olfactory sensory map develops in the absence of normal projection neurons or GABAergic interneurons. Neuron 21:1273–1282. CrossRef Medline

Cacalano G, Fariñas I, Wang LC, Hagler K, Forgie A, Moore M, Armanini M, Phillips H, Ryan AM, Reichardt LF, Hynes M, Davies A, Rosenthal A (1998) GFRalpha1 is an essential receptor component for GDNF in the

developing nervous system and kidney. Neuron 21:53–62. CrossRef Medline

Canty AJ, Dietze J, Harvey M, Enomoto H, Milbrandt J, Ibáñez CF (2009) Regionalized loss of parvalbumin interneurons in the cerebral cortex of mice with deficits in GFRalpha1 signaling. J Neurosci 29:10695–10705. CrossRef Medline

Cao L, Su Z, Zhou Q, Lv B, Liu X, Jiao L, Li Z, Zhu Y, Huang Z, Huang A, He C (2006) Glial cell line-derived neurotrophic factor promotes olfactory ensheathing cells migration. Glia 54:536–544. CrossRef Medline

Carson C, Saleh M, Fung FW, Nicholson DW, Roskams AJ (2005) Axonal dynactin p150(Glued) transports caspase-8 to drive retrograde olfactory receptor neuron apoptosis. J Neurosci 25:6092–6104. CrossRef Medline

Cho JH, Prince JE, Cutforth T, Cloutier JF (2011) The pattern of glomerular map formation defines responsiveness to aversive odorants in mice. J Neurosci 31:7920–7926. CrossRef Medline

Choi-Lundberg DL, Bohn MC (1995) Ontogeny and distribution of glial cell line-derived neurotrophic factor (GDNF) mRNA in rat. Brain Res Dev Brain Res 85:80–88. Medline

Chuah MI, West AK (2002) Cellular and molecular biology of ensheathing cells. Microsc Res Tech 58:216–227. CrossRef Medline

Cowan CM, Roskams AJ (2004) Caspase-3 and caspase-9 mediate developmental apoptosis in the mouse olfactory system. J Comp Neurol 474:136–148. CrossRef Medline

Cowan CM, Thai J, Krajewski S, Reed JC, Nicholson DW, Kaufmann SH, Roskams AJ (2001) Caspases 3 and 9 send a pro-apoptotic signal from synapse to cell body in olfactory receptor neurons. J Neurosci 21:7099–7109. Medline

D'Amelio M, Cavallucci V, Middei S, Marchetti C, Pacioni S, Ferri A, Diamantini A, De Zio D, Carrara P, Battistini L, Moreno S, Bacci A, Ammassari-Teule M, Marie H, Cecconi F (2011) Caspase-3 triggers early synaptic dysfunction in a mouse model of Alzheimer's disease. Nat Neurosci 14:69–76. CrossRef Medline

De Carlos JA, López-Mascaraque L, Valverde F (1995) The telencephalic vesicles are innervated by olfactory placode-derived cells: a possible mechanism to induce neocortical development. Neuroscience 68:1167–1178. CrossRef Medline

De Marchis S, Temoney S, Erdelyi F, Bovetti S, Bovolin P, Szabo G, Puche AC (2004) GABAergic phenotypic differentiation of a subpopulation of subventricular derived migrating progenitors. Eur J Neurosci 20:1307–1317. CrossRef Medline

Enomoto H, Araki T, Jackman A, Heuckeroth RO, Snider WD, Johnson EM Jr, Milbrandt J (1998) GFR alpha1-deficient mice have deficits in the enteric nervous system and kidneys. Neuron 21:317–324. CrossRef Medline

Farbman AI, Margolis FL (1980) Olfactory marker protein during ontogeny: immunohistochemical localization. Dev Biol 74:205–215. CrossRef Medline

Gong Q, Shipley MT (1995) Evidence that pioneer olfactory axons regulate telencephalon cell cycle kinetics to induce the formation of the olfactory bulb. Neuron 14:91–101. CrossRef Medline

Hinds JW (1968a) Autoradiographic study of histogenesis in the mouse olfactory bulb. II. Cell proliferation and migration. J Comp Neurol 134:305–322. CrossRef Medline

Hinds JW (1968b) Autoradiographic study of histogenesis in the mouse olfactory bulb. I. Time of origin of neurons and neuroglia. J Comp Neurol 134:287–304. CrossRef Medline

Hurtado-Chong A, Yusta-Boyo MJ, Vergaño-Vera E, Bulfone A, de Pablo F, Vicario-Abejón C (2009) IGF-I promotes neuronal migration and positioning in the olfactory bulb and the exit of neuroblasts from the subventricular zone. Eur J Neurosci 30:742–755. CrossRef Medline

Jain S, Golden JP, Wozniak D, Pehek E, Johnson EM Jr, Milbrandt J (2006) RET is dispensable for maintenance of midbrain dopaminergic neurons in adult mice. J Neurosci 26:11230–11238. CrossRef Medline

Kobayakawa K, Kobayakawa R, Matsumoto H, Oka Y, Imai T, Ikawa M, Okabe M, Ikeda T, Itohara S, Kikusui T, Mori K, Sakano H (2007) Innate versus learned odour processing in the mouse olfactory bulb. Nature 450:503–508. CrossRef Medline

Kramer ER, Aron L, Ramakers GM, Seitz S, Zhuang X, Beyer K, Smidt MP, Klein R (2007) Absence of Ret Signaling in Mice Causes Progressive and Late Degeneration of the Nigrostriatal System. PLoS Biol 5:e39. CrossRef Medline

Ledda F, Paratcha G, Sandoval-Guzmán T, Ibáñez CF (2007) GDNF and GFRalpha1 promote formation of neuronal synapses by ligand-induced cell adhesion. Nat Neurosci 10:293–300. CrossRef Medline

Li Z, Jo J, Jia JM, Lo SC, Whitcomb DJ, Jiao S, Cho K, Sheng M (2010) Caspase-3 activation via mitochondria is required for long-term depression and AMPA receptor internalization. Cell 141:859–871. CrossRef Medline

Lin LF, Doherty DH, Lile JD, Bektesh S, Collins F (1993) GDNF: a glial cell line-derived neurotrophic factor for midbrain dopaminergic neurons. Science 260:1130–1132. CrossRef Medline

Lois C, Alvarez-Buylla A (1994) Long-distance neuronal migration in the adult mammalian brain. Science 264:1145–1148. CrossRef Medline

Luskin MB (1993) Restricted proliferation and migration of postnatally generated neurons derived from the forebrain subventricular zone. Neuron 11:173–189. CrossRef Medline

Luskin MB (1998) Neuroblasts of the postnatal mammalian forebrain: their phenotype and fate. J Neurobiol 36:221–233. CrossRef Medline

Maroldt H, Kaplinovsky T, Cunningham AM (2005) Immunohistochemical expression of two members of the GDNF family of growth factors and their receptors in the olfactory system. J Neurocytol 34:241–255. CrossRef Medline

Miragall F, Monti Graziadei GA (1982) Experimental studies on the olfactory marker protein. II. Appearance of the olfactory marker protein during differentiation of the olfactory sensory neurons of mouse: an immunohistochemical and autoradiographic study. Brain Res 239:245–250. CrossRef Medline

Mobley AS, Miller AM, Araneda RC, Maurer LR, Müller F, Greer CA (2010) Hyperpolarization-activated cyclic nucleotide-gated channels in olfactory sensory neurons regulate axon extension and glomerular formation. J Neurosci 30:16498–16508. CrossRef Medline

Murdoch B, Roskams AJ (2007) Olfactory epithelium progenitors: insights from transgenic mice and in vitro biology. J Mol Histol 38:581–599. CrossRef Medline

Nicolay DJ, Doucette JR, Nazarali AJ (2006) Transcriptional regulation of neurogenesis in the olfactory epithelium. Cell Mol Neurobiol 26:803–821. Medline

Nikolaev A, McLaughlin T, O'Leary DD, Tessier-Lavigne M (2009) APP binds DR6 to trigger axon pruning and neuron death via distinct caspases. Nature 457:981–989. CrossRef Medline

Nosrat CA, Tomac A, Hoffer BJ, Olson L (1997) Cellular and developmental patterns of expression of Ret and glial cell line-derived neurotrophic factor receptor alpha mRNAs. Exp Brain Res 115:410–422. CrossRef Medline

Paratcha G, Ledda F, Ibáñez CF (2003) The neural cell adhesion molecule NCAM is an alternative signaling receptor for GDNF family ligands. Cell 113:867–879. CrossRef Medline

Paratcha G, Ibáñez CF, Ledda F (2006) GDNF is a chemoattractant factor for neuronal precursor cells in the rostral migratory stream. Mol Cell Neurosci 31:505–514. CrossRef Medline

Park KJ, Grosso CA, Aubert I, Kaplan DR, Miller FD (2010) p75NTR-dependent, myelin-mediated axonal degeneration regulates neural connectivity in the adult brain. Nat Neurosci 13:559–566. CrossRef Medline

Parrish-Aungst S, Shipley MT, Erdelyi F, Szabo G, Puche AC (2007) Quantitative analysis of neuronal diversity in the mouse olfactory bulb. J Comp Neurol 501:825–836. CrossRef Medline

Perrinjaquet M, Sjöstrand D, Moliner A, Zechel S, Lamballe F, Maina F, Ibáñez CF (2011) MET signaling in GABAergic neuronal precursors of the medial ganglionic eminence restricts GDNF activity in cells that express GFRα1 and a new transmembrane receptor partner. J Cell Sci 124:2797–2805. CrossRef Medline

Pichel JG, Shen L, Sheng HZ, Granholm AC, Drago J, Grinberg A, Lee EJ, Huang SP, Saarma M, Hoffer BJ, Sariola H, Westphal H (1996) Defects in enteric innervation and kidney development in mice lacking GDNF. Nature 382:73–76. CrossRef Medline

Potter SM, Zheng C, Koos DS, Feinstein P, Fraser SE, Mombaerts P (2001) Structure and emergence of specific olfactory glomeruli in the mouse. J Neurosci 21:9713–9723. Medline

Pozas E, Ibáñez CF (2005) GDNF and GFRalpha1 promote differentiation and tangential migration of cortical GABAergic neurons. Neuron 45:701–713. CrossRef Medline

Rinberg D, Koulakov A, Gelperin A (2006) Speed-accuracy tradeoff in olfaction. Neuron 51:351–358. CrossRef Medline

Schoenmann Z, Assa-Kunik E, Tiomny S, Minis A, Haklai-Topper L, Arama

E, Yaron A (2010) Axonal degeneration is regulated by the apoptotic machinery or a NAD+-sensitive pathway in insects and mammals. J Neurosci 30:6375–6386. CrossRef Medline

Tamamaki N, Yanagawa Y, Tomioka R, Miyazaki J, Obata K, Kaneko T (2003) Green fluorescent protein expression and colocalization with calretinin, parvalbumin, and somatostatin in the GAD67-GFP knock-in mouse. J Comp Neurol 467:60–79. CrossRef Medline

Treloar HB, Miller AM, Ray A, Greer CA (2009a) Development of the olfactory system. In: The Neurobiology of Olfaction (Menini A, ed), pp 131–156. Boca Raton, FL: CRC.

Treloar HB, Ray A, Dinglasan LA, Schachner M, Greer CA (2009b) Tenascin-C is an inhibitory boundary molecule in the developing olfactory bulb. J Neurosci 29:9405–9416. CrossRef Medline

Trupp M, Belluardo N, Funakoshi H, Ibáñez CF (1997) Complementary and overlapping expression of glial cell line-derived neurotrophic factor (GDNF), c-ret proto-oncogene, and GDNF receptor-alpha indicates multiple mechanisms of trophic actions in the adult rat CNS. J Neurosci 17:3554–3567. Medline

Verhaagen J, Oestreicher AB, Gispen WH, Margolis FL (1989) The expression of the growth associated protein B50/GAP43 in the olfactory system of neonatal and adult rats. J Neurosci 9:683–691. Medline

Verhaagen J, Oestreicher AB, Grillo M, Khew-Goodall YS, Gispen WH, Margolis FL (1990) Neuroplasticity in the olfactory system: differential effects of central and peripheral lesions of the primary olfactory pathway on the expression of B-50/GAP43 and the olfactory marker protein. J Neurosci Res 26:31–44. CrossRef Medline

Waclaw RR, Allen ZJ 2nd, Bell SM, Erdélyi F, Szabó G, Potter SS, Campbell K (2006) The zinc finger transcription factor Sp8 regulates the generation and diversity of olfactory bulb interneurons. Neuron 49:503–516. CrossRef Medline

Whitley M, Treloar H, De Arcangelis A, Georges Labouesse E, Greer CA (2005) The alpha6 integrin subunit in the developing mouse olfactory bulb. J Neurocytol 34:81–96. CrossRef Medline

Wichterle H, Turnbull DH, Nery S, Fishell G, Alvarez-Buylla A (2001) In utero fate mapping reveals distinct migratory pathways and fates of neurons born in the mammalian basal forebrain. Development 128:3759–3771. Medline

Windus LC, Chehrehasa F, Lineburg KE, Claxton C, Mackay-Sim A, Key B, St John JA (2011) Stimulation of olfactory ensheathing cell motility enhances olfactory axon growth. Cell Mol Life Sci 68:3233–3247. CrossRef Medline

Witt RM, Galligan MM, Despinoy JR, Segal R (2009) Olfactory behavioral testing in the adult mouse. J Vis Exp pii:949. CrossRef Medline

Yang M, Crawley JN (2009) Simple behavioral assessment of mouse olfaction. Curr Protoc Neurosci Chapter 8:Unit 8.24. Medline

Yu T, Scully S, Yu Y, Fox GM, Jing S, Zhou R (1998) Expression of GDNF family receptor components during development: implications in the mechanisms of interaction. J Neurosci 18:4684–4696. Medline